

Revisiting Data Scaling Law for Medical Segmentation

Yuetan Chu¹, Zhongyi Han¹, Gongning Luo¹(✉), and Xin Gao¹(✉)

Computational Bioscience Research Center (CBRC), King Abdullah University of
Science and Technology (KAUST), Thuwal, Saudi Arabia
{gongning.luo, xin.gao}@kaust.edu.sa

Abstract. The population loss of trained deep neural networks often exhibits power law scaling with the size of the training dataset, guiding significant performance advancements in deep learning applications. In this study, we focus on the scaling relationship with data size in the context of medical anatomical segmentation, a domain that remains underexplored. We analyze scaling laws for anatomical segmentation across 15 semantic tasks and 4 imaging modalities, demonstrating that larger datasets significantly improve segmentation performance, following similar scaling trends. Motivated by the topological isomorphism in images sharing anatomical structures, we evaluate the impact of deformation-guided augmentation strategies on data scaling laws, specifically random elastic deformation and registration-guided deformation. We also propose a novel, scalable image augmentation approach that generates diffeomorphic mappings from geodesic subspace based on image registration to introduce realistic deformation. Our experimental results demonstrate that both registered and generated deformation-based augmentation considerably enhance data utilization efficiency. The proposed generated deformation method notably achieves superior performance and accelerated convergence, surpassing standard power law scaling trends without requiring additional data. Overall, this work provides insights into the understanding of segmentation scalability and topological variation impact in medical imaging, thereby leading to more efficient model development with reduced annotation and computational costs.

Keywords: Deep learning · Scaling law · Segmentation · Registration

1 Introduction

Deep learning has achieved remarkable progress through the scaling of models, data, and computational resources. A key factor driving this advancement is the empirical observation of neural scaling laws, as the systematic relationships that describe how model performance improves as these resources expand[1]. These scaling laws, often characterized by power law relationships, have been observed across various domains, including computer vision, natural language processing,

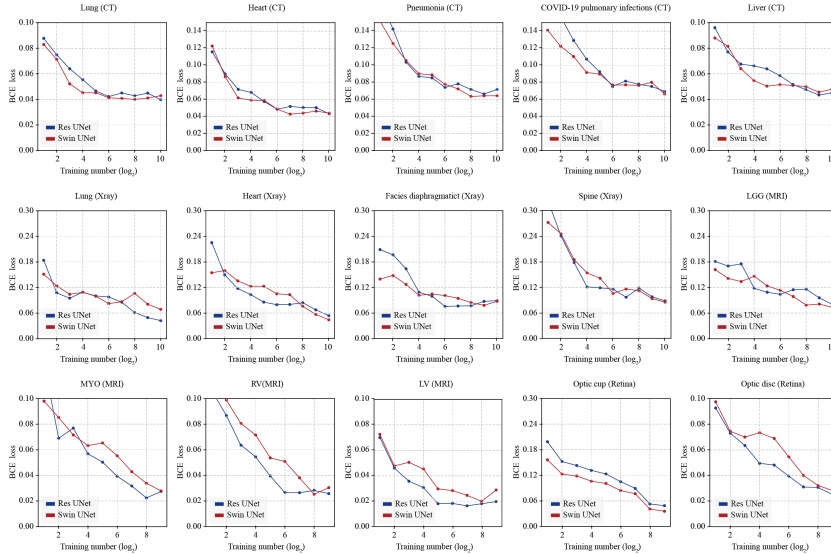


Fig. 1. Validation of data scaling law in medical segmentation tasks. We use the BCE loss as the predicted error, and employ both Res-UNet and Swin-UNet as the segmentation backbone.

and speech recognition[2], where errors decrease predictably with increases in training dataset size, model size, or computational budget. While these scaling behaviors have enabled significant achievements, such as advancements in language representation and image understanding[3], their application to image segmentation, particularly in the field of medical semantic segmentation, remains relatively underexplored. Medical image segmentation[4] is a critical deep learning application, enabling the precise identification of anatomical structures and abnormalities in medical images, which is essential for accurate diagnosis, surgical planning, and quantitative analysis in modern healthcare. Given the substantial time and labor required for detailed annotation in medical image segmentation[6], this study focuses on investigating data scaling laws to understand how segmentation performance improves with increasing training data size, providing insights to guide the development of more efficient and robust medical AI systems.

To investigate scaling laws in medical segmentation, this study conducted experiments across four major medical imaging modalities: X-ray, computed tomography (CT), magnetic resonance imaging (MRI), and retinal imaging, encompassing a total of 15 semantic segmentation tasks. By measuring predicted errors using binary cross-entropy (BCE), we observed a similar power law-driven decrease in error as the training dataset size increased, applicable to both convolutional networks (Res-UNet)[4] and Swin-UNet[5]-based networks (Fig. 1). These experiments provide initial evidence supporting the existence of data scaling laws in medical segmentation tasks. Nevertheless, they also highlight a significant challenge: achieving satisfactory segmentation performance requires an

exponential increase in training data. Given the great efforts of medical image annotation, this raises a critical research question: could we achieve more efficient scaling relationships through optimized data augmentation strategies or selective sampling approaches?

The conservative nature of human anatomy, which is characterized by consistent organ shapes and distributions across individuals, suggests that even a limited set of annotated data can capture universal anatomical patterns[7][8]. This anatomical consistency is also reflected by the success of inter-person registration algorithms, which can effectively transfer topology between samples to enhance generalizability[9][10]. Building on this premise, we investigated how deformation-based augmentation approaches could improve segmentation scaling laws. Our study examined three augmentation methods: random elastic deformation, diffeomorphic transformation based on existing data registration[11][7], and our proposed transformation based on the generated deformation field model. The experimental results demonstrate that while elastic deformation yields limited improvements, both registration-deformation augmentation (RegDA) and generated-deformation augmentation (GenDA) significantly enhance the convergence of predicted loss curves in the scaling analysis. Notably, GenDA can demonstrate superior performance and computational efficiency compared to RegDA across most scenarios. These findings suggest a promising approach for reducing the resource requirements of accurate segmentation models.

2 Scaling-law in Medical Segmentation

In this section, we conducted comprehensive experiments to validate the scaling law in medical segmentation tasks. We employed Res-UNet (feature size=32, 1.96M parameters)[4] and Swin-UNet (feature size=12, 1.59M parameters)[5] architectures. The experiments spanned four major medical imaging modalities and 15 semantic segmentation tasks, with dataset details presented in Table 1. Models were trained using the Adam optimizer with an initial learning rate of 1×10^{-4} , employing a cosine decay schedule and linear warmup over 5 epochs. The training was conducted with a batch size of 8. Input images were resized to 512×512 pixels and normalized to $[0,1]$. Baseline data augmentation included random flipping (horizontal and vertical), rotation ($\pm\pi/10$), affine transformations (scale: 0.9-1.1, shear: $\pm\pi/10$), and histogram shifting (± 0.2)[13]. Models were initialized using Xavier initialization and trained on a Linux workstation with NVIDIA A6000 (48GB). We implemented an exponential scaling protocol for the training set size, following powers of 2 [$2^0, 2^1, 2^2, 2^3, 2^4, \dots$] contingent upon the available dataset size. Each model was trained for 50 epochs with an early stopping mechanism (patience=10) monitored on validation loss. Model checkpoints were saved at the point of minimum validation loss, with validation performed after each epoch. To ensure statistical robustness, we conducted 20 independent trials for the training set sizes less than 2^4 while 10 trials for larger sets, and reported the mean performance metrics. The experimental results are presented in Fig. 1.

Modality	Dataset Name	Segmentation tasks
CT	Private dataset	Lung, heart
CT	Point-annotation segmentation[6]	Pneumonia
CT	COVID-19 Seg Challenge[14]	COVID-19 pulmonary infections
CT	Abdomen-1K[15]	Liver
Xray	Xray landmark[16]	Lung, heart
Xray	Torchxrayvision[17]	Facies diaphragmatica, spine
MRI	BraTS-TCGA-LGG[18]	Low Grade Glioma (LGG)
MRI	ACDC[19]	Left ventricle (LV), Right ventricle (RV), Myocardium (MYO)
Retinal (fundus)	RiGA[20]&PAPILA[21]	Optic disc, optic cup

Table 1. Dataset details for segmentation scaling law validation.

Fig. 1 demonstrates an overall power law scaling relationship between training dataset size and segmentation performance, with both Res-UNet and Swin-UNet models exhibiting consistent improvements as the dataset size increases. Across all tasks, BCE loss predictably decreases with larger datasets, supporting that scaling dataset size can enhance segmentation accuracy. In general, the loss exhibits a negative linear relationship with the logarithm of the training data size for most tasks, validating the power law scaling behavior. For relatively simple tasks, such as lung CT and heart CT analysis, the performance improvement of models tends to plateau as the dataset size increases, exhibiting diminishing returns. This suggests that the power law relationship between dataset size and segmentation performance may have a threshold, which likely varies depending on task complexity. This phenomenon could be attributed to two factors: first, the subjectivity of manual annotation may limit further performance gains; second, the segmentation targets are easier to identify, allowing models to learn sufficient features even from smaller datasets.

3 Revisit Scaling-law from a Topological Perspective

In this section, we examine the data scaling law when applying deformation-based augmentation approaches. We maintain all experimental settings consistent with the baseline configuration described in Section 2, while implementing these augmentation methods as external procedures.

3.1 Random Elastic Deformation

Random elastic deformation is a widely adopted data augmentation technique[12] that introduces realistic, non-linear distortions to images by applying random perturbations to a deformation grid, followed by elastic image warping. We implemented this transformation using the MONAI framework[13], with a grid spacing of (10, 10) pixels and a magnitude range of [1, 3]. The padding mode is set to zero while maintaining the default configuration for all other parameters.

3.2 Transformation based on Existing Data Registration

Unlike elastic deformation, which generates random and potentially unrealistic deformation fields, RegDA produces deformation fields through data registration. This approach was first proposed as the Brainstorm[7] and then generalized

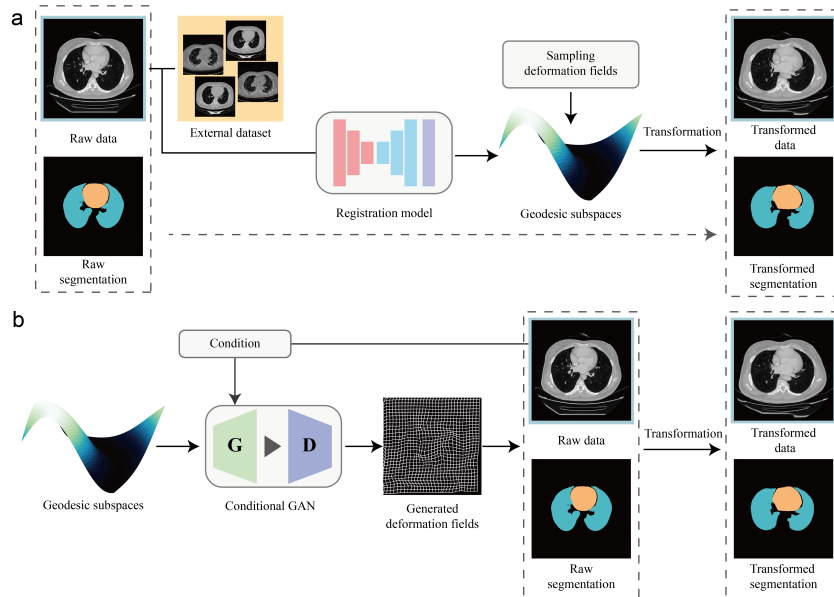


Fig. 2. The overview of RegDA and GenDA. (a) Workflow of deformation-based augmentation using registration. Deformation fields are generated by registering raw data with an external dataset, sampled from geodesic subspaces, and applied to transform the data and segmentation annotations. (b) Proposed transformation method based on generated deformation: geodesic subspaces are used to conditionally train a GAN to generate deformation fields, which are then applied to raw data and segmentation annotations for augmentation. This approach reduces reliance on external datasets.

and improved by [11], and we adopt the latter version in this study. It can enhance topological generalizability by extending the dataset topology to include data beyond the training set, while regularization and diffeomorphism in the registration ensure smooth, invertible, and topology-preserving deformation fields that yield reasonable and realistic transformations. The workflow of RegDA is presented in Fig. 2a.

Specifically, given a source image x within the training set and an external image $y \in \mathcal{Y}$ from an external set containing N images, RegDA first develops a registration model R based on the Large Deformation Diffeomorphic Metric Mapping (LDDMM) framework[25] to register x to y . This produces a corresponding deformation field $\phi_{x \rightarrow y} = R(x, y)$. LDDMM ensures that the deformation field is smooth, invertible, and anatomically plausible. The image x is then warped using the deformation field as follows:

$$\tilde{x} = x \circ \phi_{x \rightarrow y}. \quad (1)$$

where \tilde{x} is the transformed version of the source image x . In the training phase, we implement data augmentation by constructing a combined deformation field ϕ_{comb} as a convex combination of deformation fields $\phi_{x \rightarrow y_i}$, obtained by regis-

tering x to $n' \leq N$ external images $y_i \in \mathcal{Y}$. Specifically,

$$\phi_{\text{comb}} \leftarrow \sum_{i=1}^{n' < N} \lambda_i \cdot \phi_{x \rightarrow y_i} \quad (2)$$

where $\lambda_i > 0$ and $\sum_{i=1}^{n'} \lambda_i = 1$.

To ensure diffeomorphism, the deformation fields $\phi_{x \rightarrow y_i}$ are parameterized by their initial momenta. The convex combination of these momenta guarantees that the resulting transformation ϕ_{comb} remains smooth and invertible. Finally, the combined deformation field ϕ_{comb} is applied to both the source image x and its corresponding segmentation annotation s , resulting in the augmented pair (\hat{x}, \hat{s}) :

$$(\hat{x}, \hat{s}) = (x, s) \circ \phi_{\text{comb}}, \quad (3)$$

In our experimental results, we include all the data excluded from the training, validation, and test set as the external dataset \mathcal{Y} . All our processing strictly follows [11].

3.3 Proposed Methods via Generated Deformation Fields

While the RegDA method demonstrates impressive augmentation efficiency, its effectiveness is inherently constrained by external datasets. The method impact may degrade when the external datasets are limited in size or when their anatomical topologies closely resemble those in the training set. To overcome this limitation, we propose a novel approach that leverages a generative model to produce deformation fields, thereby reducing reliance on external datasets. The workflow of this approach is illustrated in Fig. 2b.

The core idea of our method is to develop a generator capable of generating new deformation fields, rather than solely relying on pre-existing external datasets. The generator is trained using deformation fields derived from the registration process between the images in the dataset. Suppose we have M images in the training set \mathcal{X} and N images in the external set \mathcal{Y} . By forming $M + N$ groups of image pairs and performing pairwise registration, we can generate up to $(M + N)^2$ deformation fields, including self-to-self identity mappings. This results in a comprehensive set of deformation fields:

$$\mathcal{P} = \{\phi_{w_i \rightarrow w_j} | w_i, w_j \in (\mathcal{X} \cup \mathcal{Y})\}. \quad (4)$$

Using this set of deformation fields, we train a conditional generative adversarial network (GAN)[22] to generate plausible deformation fields $\phi_{w_i}^G$ conditioned on a given input image w_i . The conditional GAN is implemented following [23], with additional modifications to ensure the generated deformation fields are smooth, diffeomorphic, and anatomically realistic. Specifically, we use a combination of L2-norms and the negative determinant values of the Jacobian matrices of the field[24] as the loss function in addition to the standard adversarial loss.

$$L_{\text{regu}} = \|\nabla \phi_{w_i}^G\|_2 + \text{relu}(-\det(\nabla \phi_{w_i}^G)). \quad (5)$$

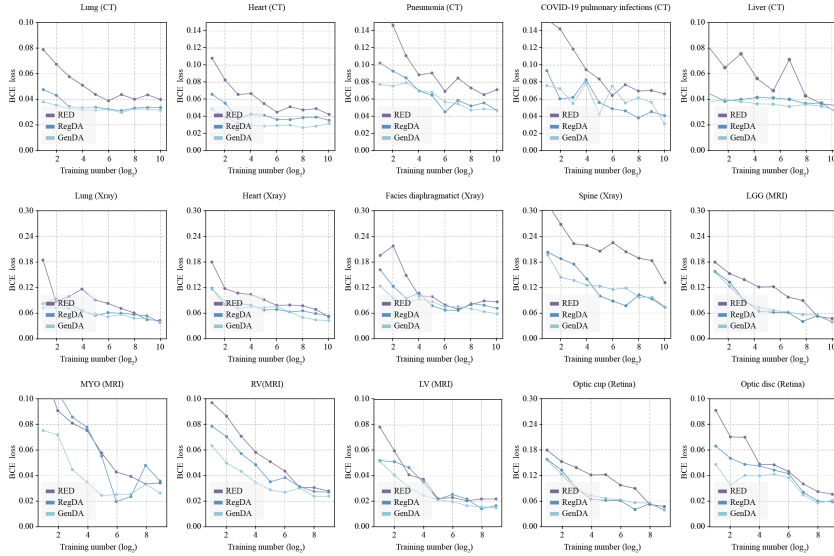


Fig. 3. Data scaling law comparison of different transformation techniques with the Res-UNet segmentation backbone. Comparison of BCE loss across various medical segmentation tasks for three methods: random elastic deformation (RED), deformation-based augmentation using RegDA, and proposed GenDA.

For the image augmentation with a training image x , we first use the generator to generate a reasonable deformation field ϕ_x^G , and then perform the transformation

$$(\hat{x}, \hat{s}) = (x, s) \circ (\mu \cdot \phi_x^G), \quad (6)$$

where $\mu \sim \text{Uniform}(0, 1)$ is the random magnitude coefficient.

3.4 Experimental results

The experimental results across different architectures (Res-UNet and Swin-UNet) are presented in Fig. 3 and 4, demonstrating the impact of various augmentation strategies on the scaling behavior of medical image segmentation. While conventional random elastic deformation shows marginal improvements over the baseline, its benefits are limited and often accompanied by increased performance variability. In contrast, both RegDA and the proposed GenDA demonstrate substantial improvements in scaling efficiency across multiple tasks and modalities, achieving significantly lower BCE loss in the low-data regime (training samples $< 2^4$) and demonstrating a clear difference from the standard logarithmic error reduction pattern. The loss curves for both methods exhibit steeper descent rates and earlier convergence compared to the power law scaling, effectively breaking the conventional scaling law limitations. Notably, GenDA consistently outperforms RegDA across most tasks, particularly in anatomically complex scenarios such as cardiac MRI and retinal imaging, which can be attributed to its ability to generate diverse yet anatomically plausible deformations

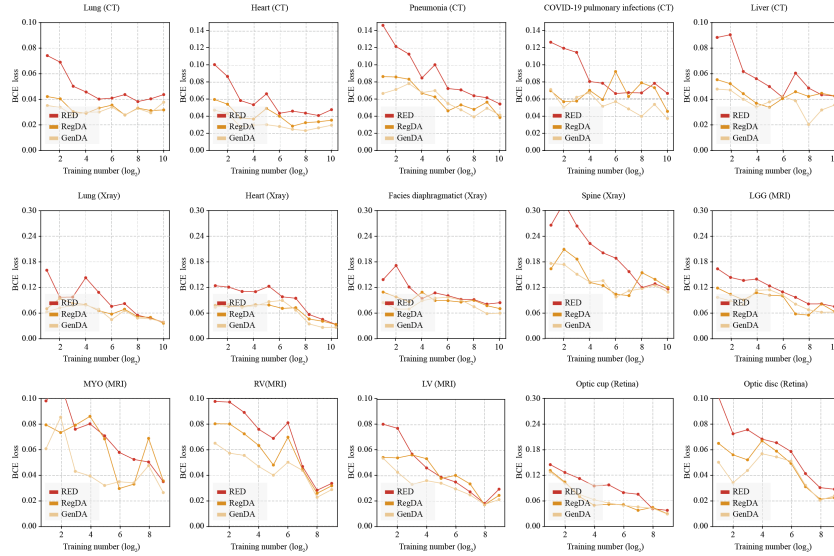


Fig. 4. Data scaling law comparison of different transformation techniques with the Swin-UNet segmentation backbone. Comparison of BCE loss across various medical segmentation tasks for three methods: random elastic deformation (RED), deformation-based augmentation using RegDA and proposed GenDA.

without relying on external reference data. These findings suggest that topology-aware augmentation strategies can effectively modify the traditional power law scaling relationship in medical image segmentation, potentially reducing the annotation burden in medical imaging applications.

4 Discussion and Conclusion

In this manuscript, we first provide comprehensive empirical evidence that medical segmentation follows data power law scaling behavior across diverse imaging modalities and anatomical structures, establishing a quantitative framework for understanding data requirements in medical AI development. We also demonstrate that topology-aware augmentation strategies can effectively break this conventional scaling law, achieving superior performance with significantly less training data. Our proposed GenDA method, in particular, shows that leveraging anatomical consistency through learned deformation fields can better improve the relationship between dataset size and model performance. Our study also exhibits some limitations, for example, the experiments were done in a 2D context, while extending to the 3D volume segmentation will be validated in our future work. Moreover, the generalization to more variable pathological conditions is still worth exploring. Collectively, our study suggests a promising direction for developing efficient medical segmentation models while reducing the burden of data annotation in clinical applications.

References

1. Kaplan, Jared, et al. "Scaling laws for neural language models." arXiv preprint arXiv:2001.08361 (2020).
2. Dosovitskiy, Alexey, et al. "An image is worth 16x16 words: Transformers for image recognition at scale." arXiv preprint arXiv:2010.11929 (2020).
3. Bahri, Yasaman, et al. "Explaining neural scaling laws." *Proceedings of the National Academy of Sciences* 121.27 (2024): e2311878121.
4. Ronneberger, Olaf, Philipp Fischer, and Thomas Brox. "U-net: Convolutional networks for biomedical image segmentation." *Medical image computing and computer-assisted intervention—MICCAI 2015: 18th international conference, Munich, Germany, October 5-9, 2015, proceedings, part III* 18. Springer international publishing, 2015.
5. Cao, Hu, et al. "Swin-UNet: Unet-like pure transformer for medical image segmentation." *European conference on computer vision*. Cham: Springer Nature Switzerland, 2022.
6. Chu, Yuetan, et al. "Point-annotation supervision for robust 3D pulmonary infection segmentation by CT-based cascading deep learning." *Computers in Biology and Medicine* 187 (2025): 109760.
7. Zhao, Amy, et al. "Data augmentation using learned transformations for one-shot medical image segmentation." *Proceedings of the IEEE/CVF conference on computer vision and pattern recognition*. 2019.
8. Chu, Yuetan, et al. "Anatomic-Constrained Medical Image Synthesis via Physiological Density Sampling." *International Conference on Medical Image Computing and Computer-Assisted Intervention*. Cham: Springer Nature Switzerland, 2024.
9. Balakrishnan, Guha, et al. "Voxelmorph: a learning framework for deformable medical image registration." *IEEE transactions on medical imaging* 38.8 (2019): 1788-1800.
10. Ou, Zhuolin, Xiaoqi Lu, and Yu Gu. "HCS-Net: Multi-level deformation strategy combined with quadruple attention for image registration." *Computers in Biology and Medicine* 168 (2024): 107832.
11. Shen, Zhengyang, et al. "Anatomical data augmentation via fluid-based image registration." *Medical Image Computing and Computer Assisted Intervention—MICCAI 2020: 23rd International Conference, Lima, Peru, October 4–8, 2020, Proceedings, Part III* 23. Springer International Publishing, 2020.
12. Zhang, Xuechen, et al. "DCES-PA: Deformation-controllable elastic shape model for 3D bone proliferation analysis using hand HR-pQCT images." *Computers in Biology and Medicine* 175 (2024): 108533.
13. Diaz-Pinto, Andres, et al. "Monai label: A framework for ai-assisted interactive labeling of 3d medical images." *Medical Image Analysis* 95 (2024): 103207.
14. H. R. Roth, Z. Xu, C. Tor-Diez, R. S. Jacob, J. Zember, J. Molto, W. Li, S. Xu, B. Turkbey, E. Turkbey et al., "Rapid artificial intelligence solutions in a pandemic—the covid-19-20 lung ct lesion segmentation challenge," *Medical Image Analysis*, vol. 82, p. 102605, 2022.
15. Ma, Jun, et al. "Abdomenct-1k: Is abdominal organ segmentation a solved problem?." *IEEE Transactions on Pattern Analysis and Machine Intelligence* 44.10 (2021): 6695-6714.
16. Gaggion, Nicolás, Lucas Mansilla, Candelaria Mosquera, Diego H. Milone, and Enzo Ferrante. "Improving anatomical plausibility in medical image segmentation via hybrid graph neural networks: applications to chest x-ray analysis." *IEEE Transactions on Medical Imaging* 42, no. 2 (2022): 546-556.

17. Cohen, Joseph Paul, et al. "TorchXRyVision: A library of chest X-ray datasets and models." International Conference on Medical Imaging with Deep Learning. PMLR, 2022.
18. Pedano, Nancy, Adam E. Flanders, Lisa Scarpace, Tom Mikkelsen, Jennifer M. Eschbacher, Beth Hermes, Victor Sisneros, Jill Barnholtz-Sloan, and Quinn Ostrom. "The cancer genome atlas low grade glioma collection (TCGA-LGG)." (2016).
19. O. Bernard, A. Lalande, C. Zotti, F. Cervenansky, et al. "Deep Learning Techniques for Automatic MRI Cardiac Multi-structures Segmentation and Diagnosis: Is the Problem Solved ?" in IEEE Transactions on Medical Imaging, vol. 37, no. 11, pp. 2514-2525, Nov. 2018
20. Eslami, M., Motati, L.S., Kalahasty, R., Hashemabad, S.K., Shi, M., Luo, Y., Tian, Y., Zebardast, N., Wang, M. and Elze, T., 2023. Deep Learning based Adversarial Disturbances in Fundus Image Analysis. Investigative Ophthalmology Visual Science, 64(9), pp.PB002-PB002.
21. O. Kovalyk, J. Morales-Sanchez, R. Verddu-Monedero, I. Selles-Navarro, A. Palazon-Cabanes, and J.-L. Sancho-Gomez, "Papila: Dataset with fundus images and clinical data of both eyes of the same patient for glaucoma assessment," Scientific Data, vol. 9, no. 1, p. 291, 2022.
22. Mirza, Mehdi, and Simon Osindero. "Conditional generative adversarial nets." arXiv preprint arXiv:1411.1784 (2014).
23. Hamghalam, Mohammad, and Amber L. Simpson. "Medical image synthesis via conditional GANs: Application to segmenting brain tumours." Computers in Biology and Medicine 170 (2024): 107982.
24. Dai, Linrui, et al. "GuideGen: A Text-Guided Framework for Full-torso Anatomy and CT Volume Generation." arXiv preprint arXiv:2403.07247 (2024).
25. Christensen, Gary E., Richard D. Rabbitt, and Michael I. Miller. "Deformable templates using large deformation kinematics." IEEE transactions on image processing 5.10 (1996): 1435-1447.